Received: 24 February 2023 | Revised: 5 July 2023 | Accepted: 17 July 2023

DOI: 10.4218/etrij.2023-0075

ETRI Journal WILEY

ORIGINAL ARTICLE

Direct position tracking method for non-circular signals with distributed passive arrays via first-order approximation

Jinke Cao[1,2] | **Xiaofei Zhang**[1,2] | **Honghao Hao**[1,2]

[1]College of Electronic and Information Engineering, Nanjing University of Aeronautics and Astronautics, Nanjing, China

[2]Key Laboratory of Dynamic Cognitive System of Electromagnetic Spectrum Space (Nanjing University of Aeronautics and Astronautics), Ministry of Industry and Information Technology, Nanjing, China

Correspondence
Jinke Cao, College of Electronic and Information Engineering, Nanjing University of Aeronautics and Astronautics, Nanjing, 211106, China.
Email: caojinke@nuaa.edu.cn

Abstract

In this study, a direct position tracking method for non-circular (NC) signals using distributed passive arrays is proposed. First, we calculate the initial positions of sources using a direct position determination (DPD) approach; next, we transform the tracking into a compensation problem. The offsets of the adjacent time positions are calculated using a first-order Taylor expansion. The fusion calculation of the noise subspace is performed according to the NC characteristics. Because the proposed method uses the signal information from the previous iteration, it can realize automatic data associations. Compared with traditional DPD and two-step localization methods, our novel process has lower computational complexity and provides higher accuracy. Moreover, its performance is better than that of the traditional tracking methods. Numerous simulation results support the superiority of our proposed method.

KEYWORDS

direct position determination, direct tracking, distributed passive array, non-circular signal, subspace, Taylor expansion

1 | INTRODUCTION

Wireless tracking is an important research topic in array signal processing; it is widely used in radar, communication, and vehicular engineering applications [1, 2]. The common two-step method [3], which comprises two independent steps, is used for tracking the position of a source. In these methods, first, the position parameters (e.g., direction of arrival [DOA] [4], Doppler frequency shift [5], and time difference of arrival [TDOA] [6]) of the target source are measured. Subsequently, these parameters are used to calculate source locations, essentially ignoring the fact that all receivers simultaneously intercept the same transmitted signal. Additionally, these methods have been shown to be suboptimal for sensor array-based localization. Therefore, two-step localization algorithms suffer from poor accuracy at low signal-to-noise ratios (SNRs), and their computational complexity increases geometrically with the number of sources [7].

By contrast, the one-step direct position determination (DPD) method [8] has significant advantages because it directly tracks sources by constructing a cost function. By avoiding the construction of geometric relationships, the DPD method is more adaptable to low SNR and produces more accurate results [9]. The first precise maximum likelihood-based DPD technique [10] for single emitters was developed in 2004; hence, the

application of DPD to numerous localization scenarios has been extensively studied. Specifically, Demissie et al. proposed a moving single-array DPD technique [11] in 2008, which obtains source locations via subspace data fusion (SDF). Another common DPD approach is to receive signals through multiple fixed-location stations and transmit them to a fusion center (FC) [12, 13], whereas the positioning procedure is performed only at the FC. However, FC-based algorithms require higher communication bandwidths [14]. Tirer and Weiss [15] introduced an algorithm that does not require foreknowledge of emitted signals types, which reduces computational burdens. Additionally, because the FC-based DPD algorithm processes all receiver intercepts simultaneously, it exhibits more robust performance than single-station DPD algorithms [16]. However, the drawback of the DPD algorithm is that its complexity is so high that it prevents real-time tracking.

Conventional DPD methods are based on circular signals. However, non-circular (NC) signals vary in terms of the elliptical covariance. NC signals are often used in digital modulation schemes, such as binary phase shift keying (BPSK) [17] and amplitude-shift keying (ASK) [18]. Therefore, the NC signal position must be estimated. Based on the SDF algorithm, [19] proposed a DPD method for NC signals using a uniform line array (ULA) that provides significant improvements in emitter position and number estimation accuracy over traditional circular signal algorithms. DPD methods for NC signals with moving coprime and nested arrays were examined in [20] and [21], respectively, which further improved the performance in locating NC signals. For practical situations, [22] proposed a DPD method for NC signals using self-calibration techniques in the presence of mutual coupling. Despite the advances in DPD methods for NC signals, their complexity has not been reduced and they still present significant shortcomings in tracking.

To better track NC signals, we developed a novel DPT technique. Our main contributions are as follows.

1. Our proposed method for solving the position-tracking problem of NC signals from distributed passive arrays lacks the conventional repetitive (two-step) DOA and position estimation (DPD) methods in which successive sets of estimates provide the tracking trajectory. Instead, it avoids repeated calculations and tracks both position and NC phase iteratively.
2. To realize low-complexity tracking and automatic data associations, we use Taylor expansions to transform tracking tasks into compensation problems to ensure that multiple sources can be tracked by calculating the position differences between adjacent moments. We use multi-subspace data fusion to calculate the differences, thus rendering this method more accurate than traditional versions, particularly at low SNRs. An ordinary least squares (OLS) method is used to improve performance when the source trajectories are crossed.
3. Superiority is confirmed via complexity analyses and comprehensive numerical results in terms of computational complexity and tracking accuracy.

The remainder of this paper is organized as follows. Section 2 introduce the tracking model and the NC sources. Section 3 describes the processing of the received signal using the proposed algorithm. Section 4 presents a performance analysis, which includes complexity and simulation analyses. Finally, Section 5 presents the concluding remarks.

Notation: $(\cdot)^{\mathrm{T}}$, $(\cdot)^{\mathrm{H}}$, $(\cdot)^*$, and $(\cdot)^+$ represent transposition, conjugate-transpose, conjugation-and-pseudo-inverse operations, respectively. $\otimes$ is the Kronecker product, and $\mathrm{E}(\cdot)$ represents the expanded range. $||\cdot||$ is the Euclidean norm, $\mathbf{O}_{m\times n}$ represents a zero matrix, $m \times n$, and $\partial(\cdot)$ denotes a partial derivative. $\tilde{p}$ represents an estimate of p.

2 | SIGNAL AND SYSTEM MODEL

As seen in Figure 1, we consider a two-dimensional position tracking scenario. Assuming there are K far-field narrowband moving NC signals incoherently impinging onto L observation stations equipped with a ULA, the position of the kth signal at time t is $\mathbf{p}_{k,t} = (x_{k,t}, y_{k,t})^{\mathrm{T}} (k = 1, 2, \cdots, K)$. Observation stations are situated at $\mathbf{u}_l = (x_l, y_l)^{\mathrm{T}} (l = 1, 2, \cdots, L)$, and we assume that all stations are time-synchronized. The received signal at the lth station can be expressed as follows [23].

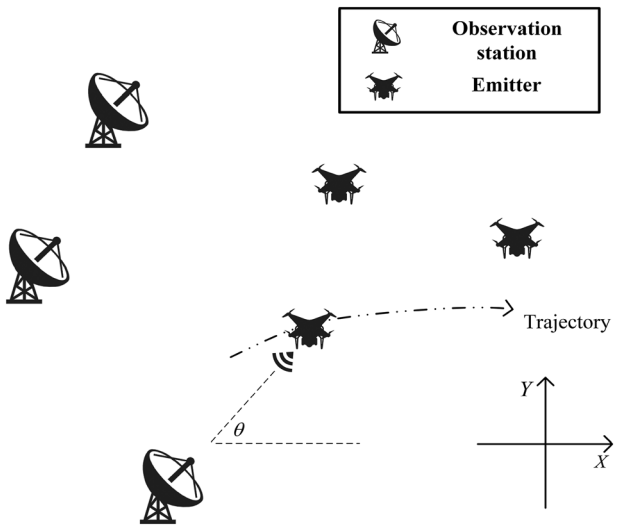

FIGURE 1 Tracking scenario.

$$\mathbf{X}_l(t) = \mathbf{A}_l(t)\mathbf{S}_l(t) + \mathbf{n}_l(t), \tag{1}$$

where $t = 1, 2, \cdots, N_S$, and N_S is the total observation time. $\mathbf{A}_l(t)$ denotes the steering matrix, which is given by

$$\mathbf{A}_l(t) = [\mathbf{a}_{l,1}(t), \mathbf{a}_{l,2}(t), \cdots, \mathbf{a}_{l,K}(t)]. \tag{2}$$

The steering vector, $\mathbf{a}_{l,k}(t)$, is

$$\mathbf{a}_{l,k}(t) = \left[1, e^{-j\frac{2\pi}{\lambda}dq_{l,k}(t)}, \cdots, e^{-j\frac{2\pi}{\lambda}d(M-1)q_{l,k}(t)}\right]^{\mathrm{T}}, \tag{3}$$

where $q_{l,k}(t) = (y_{k,t} - y_l)/||(x_{k,t} - x_l), (y_{k,t} - y_l)||$ and λ represents the wavelength of the impinging signals. M and d are the number of antennas and array spacings, respectively. The signal matrix is

$$\mathbf{S}_l(t) = [\mathbf{s}_{l,1}(t), \cdots, \mathbf{s}_{l,k}(t), \cdots, \mathbf{s}_{l,K}(t)]^{\mathrm{T}} \in \mathbb{C}^{K\times J}, \tag{4}$$

where J is the number of snapshots, and

$$\mathbf{s}_{l,k}(t) = \bar{\mathbf{s}}_{l,k}(t)e^{j\varphi_k} \in \mathbb{C}^{1\times J} \tag{5}$$

denotes the NC signal from the kth emitter received by the lth station at time t. $\bar{\mathbf{s}}_{l,k}(t)$ is the amplitude vector of the kth signal, and φ_k is the NC phase. Thus, the signal matrix can be written as

$$\mathbf{S}_l(t) = \mathbf{\Omega}\bar{\mathbf{s}}_l(t), \tag{6}$$

where

$$\mathbf{\Omega} = \begin{bmatrix} e^{j\varphi_1} & 0 & \cdots & 0 \\ 0 & e^{j\varphi_2} & \cdots & 0 \\ \vdots & \vdots & \ddots & \vdots \\ 0 & 0 & \cdots & e^{j\varphi_K} \end{bmatrix}, \tag{7}$$

$$\bar{\mathbf{s}}_l(t) = [\bar{\mathbf{s}}_{l,1}(t), \cdots, \bar{\mathbf{s}}_{l,k}(t), \cdots, \bar{\mathbf{s}}_{l,K}(t)]^{\mathrm{T}}. \tag{8}$$

$\bar{\mathbf{s}}_l(t)$ is a matrix of real numbers, and the received signal, $\mathbf{x}_l(t)$, can be rewritten as follows.

$$\mathbf{X}_l(t) = \mathbf{A}_l(t)\mathbf{\Omega}\bar{\mathbf{s}}_l(t) + \mathbf{n}_l(t). \tag{9}$$

$\mathbf{n}_l(t)$ is assumed to be uncorrelated with the white complex Gaussian noise with zero mean.

3 | PROPOSED METHOD

In this section, our new direct position-tracking algorithm for NC signals, which achieves position tracking through a joint multi-station Taylor expansion approximation, is described.

3.1 | Initial position estimation

NC signals preserve more useful information than circular signals. Thus, employing the NC properties of the received signal can significantly increase estimation accuracy. The received signal matrix of the lth observation station can be extended as follows [24].

$$\begin{aligned}\mathbf{z}_l(t) &= \begin{bmatrix} \mathbf{X}_l(t) \\ \mathbf{X}_l^*(t) \end{bmatrix} = \begin{bmatrix} \mathbf{A}_l(t)\mathbf{\Omega} \\ \mathbf{A}_l^*(t)\mathbf{\Omega}^* \end{bmatrix}\bar{\mathbf{s}}_l(t) + \begin{bmatrix} \mathbf{n}_l(t) \\ \mathbf{n}_l^*(t) \end{bmatrix} \\ &= \mathbf{B}_l(t)\bar{\mathbf{s}}_l(t) + \bar{\mathbf{n}}_l(t),\end{aligned} \tag{10}$$

where the extended steering matrix is

$$\mathbf{B}_l(t) = \begin{bmatrix} \mathbf{A}_l(t)\mathbf{\Omega} \\ \mathbf{A}_l^*(t)\mathbf{\Omega}^* \end{bmatrix} = [\mathbf{b}_{l,1}(t), \cdots, \mathbf{b}_{l,K}(t)]. \tag{11}$$

The extended steering vector is expressed as

$$\begin{aligned}\mathbf{b}_{l,k}(t) = \Big[&e^{-j\varphi_k}, e^{-j\left[\frac{2\pi}{\lambda}dq_{l,k}(t)+\varphi_k\right]}, \cdots, e^{-j\left[\frac{2\pi}{\lambda}d(M-1)q_{l,k}(t)+\varphi_k\right]}, \\ &e^{j\varphi_k}, e^{j\left[\frac{2\pi}{\lambda}dq_{l,k}(t)+\varphi_k\right]}, \cdots, e^{j\left[\frac{2\pi}{\lambda}d(M-1)q_{l,k}(t)+\varphi_k\right]}\Big]^{\mathrm{T}}.\end{aligned} \tag{12}$$

The complex Gaussian noise vector is $\bar{\mathbf{n}}_l(t) = \begin{bmatrix} \mathbf{n}_l(t) \\ \mathbf{n}_l^*(t) \end{bmatrix}$, and its noise power is σ_n^2. The covariance matrix of the received signal can be calculated as

$$\mathbf{R}_l(t) = \mathrm{E}\left[\mathbf{z}_l(t)\mathbf{z}_l^{\mathrm{H}}(t)\right]. \tag{13}$$

In practice, (13) is not available, and the covariance matrix can be estimated from J snapshots, as follows.

$$\tilde{\mathbf{R}}_l(t) \approx \frac{1}{J}\sum\nolimits_{i=1}^{J}\mathbf{z}_{l,i}(t)\mathbf{z}_{l,i}^{\mathrm{H}}(t), \tag{14}$$

where $\mathbf{z}_{l,i}(t)$ indicates the ith snapshot of $\mathbf{z}_l(t)$. The eigenvalue decomposition of covariance matrix $\mathbf{R}_l(t)$ can be expressed as follows.

$$\mathbf{R}_l(t) = [\mathbf{U}_{l,S}(t)\mathbf{U}_{l,N}(t)]\boldsymbol{\Lambda}_l(t)[\mathbf{U}_{l,S}(t)\mathbf{U}_{l,N}(t)]^{\mathrm{H}}, \tag{15}$$

where $\mathbf{U}_{l,S}(t)$ and $\mathbf{U}_{l,N}(t)$ are the signal and noise subspaces, respectively, of the signal received by the lth observation at time t. The signal subspace consists of eigenvectors corresponding to larger K eigenvalues, and the noise subspace is composed of the remaining $2M-K$ eigenvectors. $\boldsymbol{\Lambda}_l(t)$ is a diagonal matrix comprising the eigenvalues of $\mathbf{R}_l(t)$ at time t. According to the SDF algorithm, the cost function for the NC signals is [21]

$$f(\mathbf{p},\varphi) = \sum_{l=1}^{L} ||\mathbf{U}_{l,N}^{\mathrm{H}}(t)\mathbf{b}_l(\mathbf{p},\varphi)||, \tag{16}$$

where $\mathbf{p} = (x, y)^{\mathrm{T}}$ denotes the coordinates of the position in the monitoring area and φ is the NC phase in the search range. The measurement positions of target sources $\tilde{\mathbf{p}}_{k,t}$ are obtained by searching the spectral peaks of the minimum points. The NC phases of the sources can be obtained using a one-dimensional search based on measured positions $\tilde{\mathbf{p}}_{k,t}$ and (16).

3.2 | Taylor expansion approximation-based DPT

Considering the low-speed movement of the sources, the difference in positions at adjacent times is bounded. Therefore, the source positions can be tracked by calculating the deviation. The position of a source at time $t+1$ is related to that at time t, as follows.

$$\begin{aligned} x_{k,t+1} &= x_{k,t} + \xi_{x,k,t+1}, \\ y_{k,t+1} &= y_{k,t} + \xi_{y,k,t+1}, \end{aligned} \tag{17}$$

where $\xi_{x,k,t+1}$ and $\xi_{y,k,t+1}$ are the corresponding differences in coordinates. Meanwhile, we consider that the results of the NC phase in the measurement are not completely accurate, which implies the following.

$$\varphi_{k,t+1} = \varphi_{k,t} + \xi_{\varphi,k,t+1}, \tag{18}$$

where $\xi_{\varphi,k,t+1}$ is the difference between NC phases at adjacent times. The first-order Taylor expansion of the extended steering vector, (12), at time $t+1$ is as follows.

$$\begin{aligned} &\mathbf{b}_{l,k}(t+1) \approx \\ &\mathbf{b}_{l,k}(t) + \frac{\partial \mathbf{b}_{l,k}(t)}{\partial x_{k,t}}\xi_{x,k,t+1} + \frac{\partial \mathbf{b}_{l,k}(t)}{\partial y_{k,t}}\xi_{y,k,t+1} + \frac{\partial \mathbf{b}_{l,k}(t)}{\partial \varphi_{k,t}}\xi_{\varphi,k,t+1}. \end{aligned} \tag{19}$$

Because the noise subspace is orthogonal to the steering vector [21], we obtain

$$\mathbf{U}_{l,N}^{\mathrm{H}}(t+1)\mathbf{b}_{l,k}(t+1) = \mathbf{O}_{(2M-K)\times 1}, \tag{20}$$

where $\mathbf{U}_{l,N}(t+1)$ is the noise subspace of the received signal at the lth observation station. In case of multiple sources, the orthogonality can be expressed as

$$\mathbf{U}_{l,N}^{\mathrm{H}}(t+1)\mathbf{B}_l(t+1) = \mathbf{O}_{(2M-K)\times K}. \tag{21}$$

We define the three deviation matrices as follows.

$$\boldsymbol{\xi}_x(t+1) \triangleq \begin{bmatrix} \xi_{x,1,t+1} & 0 & \cdots & 0 \\ 0 & \xi_{x,2,t+1} & \ddots & 0 \\ \vdots & \vdots & \ddots & \vdots \\ 0 & 0 & \cdots & \xi_{x,K,t+1} \end{bmatrix}, \tag{22}$$

$$\boldsymbol{\xi}_y(t+1) \triangleq \begin{bmatrix} \xi_{y,1,t+1} & 0 & \cdots & 0 \\ 0 & \xi_{y,2,t+1} & \ddots & 0 \\ \vdots & \vdots & \ddots & \vdots \\ 0 & 0 & \cdots & \xi_{y,K,t+1} \end{bmatrix}, \tag{23}$$

$$\boldsymbol{\xi}_\varphi(t+1) \triangleq \begin{bmatrix} \xi_{\varphi,1,t+1} & 0 & \cdots & 0 \\ 0 & \xi_{\varphi,2,t+1} & \ddots & 0 \\ \vdots & \vdots & \ddots & \vdots \\ 0 & 0 & \cdots & \xi_{\varphi,K,t+1} \end{bmatrix}. \tag{24}$$

Therefore, according to (11), (19), and (21), the deviation matrices satisfy the following equations.

$$\begin{aligned} &\mathbf{U}_{l,N}^{\mathrm{H}}(t+1)\mathbf{B}_l(t) + \mathbf{U}_{l,N}^{\mathrm{H}}(t+1)\partial\mathbf{B}_l(t)\begin{bmatrix} \boldsymbol{\xi}_x(t+1) \\ \boldsymbol{\xi}_y(t+1) \\ \boldsymbol{\xi}_\varphi(t+1) \end{bmatrix} \\ &\qquad = \mathbf{O}_{(2M-K)\times K}, \end{aligned} \tag{25}$$

where the partial derivative matrix, $\partial\mathbf{B}_l(t)$, is defined as

$$\partial \mathbf{B}_l(t) = \left[\frac{\partial \mathbf{B}_l(t)}{\partial x_t} \quad \frac{\partial \mathbf{B}_l(t)}{\partial y_t} \quad \frac{\partial \mathbf{B}_l(t)}{\partial \varphi_t} \right]. \tag{26}$$

According to (21) and (25), the deviation matrices can be expressed as

$$\begin{bmatrix} \boldsymbol{\xi}_x(t+1) \\ \boldsymbol{\xi}_y(t+1) \\ \boldsymbol{\xi}_\phi(t+1) \end{bmatrix} = -\boldsymbol{\mu}^{+}\boldsymbol{\nu}, \tag{27}$$

where

$$\boldsymbol{\mu} = \begin{bmatrix} \mathbf{U}_{1,N}^{\mathrm{H}}(t+1)\partial \mathbf{B}_1(t) \\ \mathbf{U}_{2,N}^{\mathrm{H}}(t+1)\partial \mathbf{B}_2(t) \\ \vdots \\ \mathbf{U}_{L,N}^{\mathrm{H}}(t+1)\partial \mathbf{B}_L(t) \end{bmatrix}, \tag{28}$$

$$\boldsymbol{\nu} = \begin{bmatrix} \mathbf{U}_{1,N}^{\mathrm{H}}(t+1)\mathbf{B}_1(t) \\ \mathbf{U}_{2,N}^{\mathrm{H}}(t+1)\mathbf{B}_2(t) \\ \vdots \\ \mathbf{U}_{L,N}^{\mathrm{H}}(t+1)\mathbf{B}_L(t) \end{bmatrix}. \tag{29}$$

Thus, offsets $\xi_{x,k,t+1}$, $\xi_{y,k,t+1}$, $\xi_{\varphi,k,t+1}$ can be calculated, and the positions and NC phases of the sources at time $t+1$ can be obtained as follows.

$$\begin{aligned} \tilde{x}_{k,t+1} &= x_{k,t} + \xi_{x,k,t+1}, \\ \tilde{y}_{k,t+1} &= y_{k,t} + \xi_{y,k,t+1}, \\ \tilde{\varphi}_{k,t+1} &= \varphi_{k,t} + \xi_{\varphi,k,t+1}. \end{aligned} \tag{30}$$

The results are then iterated to achieve the position tracking of multiple emitters. This method avoids data associations and directly calculates the position without establishing new geometric relationships. However, when the trajectories of the sources cross, position estimates at nearby points are commonly blurred, which is a problem that must be overcome. To do so, we adopt an OLS method assuming that the source position measurements at the previous m times are $\tilde{\mathbf{p}}_{k,t-m+1}$, $\tilde{\mathbf{p}}_{k,t-m+2}$, $\cdots$, $\tilde{\mathbf{p}}_{k,t}$. Next, we fit them to a polynomial. This polynomial is subsequently used to predict the position of the kth target at time $t+1$. If the position measurement of the proposed method differs considerably from the predicted position, the predicted position is used instead of the measured position. This effectively minimizes errors.

3.3 | Detailed steps for implementing the proposed methodology

The detailed steps of the proposed method are as follows.

Step 1. Use the SDF algorithm to determine the initial coordinates of sources and related NC phases.
Step 2. Calculate the covariance matrix, $\mathbf{R}_l(t+1)$, of signals received by each observation station at time $t+1$.
Step 3. Obtain the noise subspace, $\mathbf{U}_{l,N}^{\mathrm{H}}(t+1)$, by performing an eigenvalue decomposition of the covariance matrix.
Step 4. Perform Taylor expansion of the extended steering vector, $\mathbf{b}_{l,k}(t+1)$.
Step 5. Construct matrices $\boldsymbol{\mu}$ and $\mathbf{v}$ according to (28) and (29), respectively.
Step 6. Determine the deviations in accordance with (27).
Step 7. Obtain signal positions by (30).
Step 8. Repeat Steps 2–7 to achieve tracking of the signals at each time.

4 | PERFORMANCE ANALYSIS

In this section, we analyze the Cramér–Rao bound (CRB) of the proposed method and highlight its advantages in terms of complexity and simulation performance.

4.1 | CRB analysis

The CRB establishes a lower bound for the variance of an unbiased estimator and is commonly used to evaluate algorithm performance. In this section, we analyze the CRB at tracking time t. If all unknown real parameters are represented by the vector, $\boldsymbol{\gamma}$, then

$$\boldsymbol{\gamma} = \left[\mathbf{p}_x^{\mathrm{T}}, \mathbf{p}_y^{\mathrm{T}}, \boldsymbol{\Phi}^{\mathrm{T}}, \boldsymbol{\eta}^{\mathrm{T}}, \sigma_n^2 \right]^{\mathrm{T}}, \tag{31}$$

where

$$\mathbf{p}_x = [x_{1,t}, \cdots, x_{K,t}]^{\mathrm{T}}, \tag{32}$$

$$\mathbf{p}_y = [y_{1,t}, \cdots, y_{K,t}]^{\mathrm{T}}, \tag{33}$$

$$\boldsymbol{\Phi} = [\varphi_1, \cdots, \varphi_K]^{\mathrm{T}}, \tag{34}$$

$$\boldsymbol{\eta} = \left[\mathbf{c}_1^{\mathrm{T}}, \cdots, \mathbf{c}_l^{\mathrm{T}}, \cdots, \mathbf{c}_L^{\mathrm{T}} \right], \tag{35}$$

$$\mathbf{c}_l = \left[\sigma_{l,1}^2, \cdots, \sigma_{l,k}^2, \cdots, \sigma_{l,K}^2\right]^{\mathrm{T}}, \tag{36}$$

where $\sigma_{l,k}^2$ represents the power of the kth signal received by the lth observation station.

For generality and ease of exposure, we define the following.

$$\mathbf{z}_{l,i} \triangleq \mathbf{z}_{l,i}(t), \tag{37}$$

$$\mathbf{R}_l \triangleq \mathbf{R}_l(t), \tag{38}$$

$$\mathbf{p} \triangleq \left[\mathbf{p}_x^{\mathrm{T}}, \mathbf{p}_y^{\mathrm{T}}\right]^{\mathrm{T}}, \tag{39}$$

$$\boldsymbol{\upsilon} \triangleq \left[\boldsymbol{\Phi}^{\mathrm{T}}, \boldsymbol{\eta}^{\mathrm{T}}, \sigma_n^2\right]^{\mathrm{T}}. \tag{40}$$

According to [25-27], $\mathbf{z}_{l,i}(i=1, \cdots, J)$ follows an NC Gaussian distribution with a zero mean and a variance of $\mathbf{R}_l$. The logarithmic likelihood function can be expressed as

$$f(\boldsymbol{\gamma}) = \frac{J}{2}\sum_{l=1}^{L}\left(\ln(\det\{\mathbf{R}_l\} + \mathrm{tr}\{\overset{-1}{\mathbf{R}}_l \mathbf{R}_l\})\right). \tag{41}$$

All elements of the Fisher information matrix are denoted as

$$\begin{aligned}[\mathbf{J}]_{p,j} &= \frac{J}{2}\sum_{l=1}^{L}\left(\frac{\partial \mathbf{r}_l}{\partial \gamma_p}\right)^{\mathrm{H}}\left((\mathbf{R}_l)^{-T} \otimes (\mathbf{R}_l)^{-1}\right)\left(\frac{\partial \mathbf{r}_l}{\partial \gamma_j}\right) \\ &= \frac{J}{2}\sum_{l=1}^{L}\left(\frac{\partial \mathbf{r}_l'}{\partial \gamma_p}\right)^{\mathrm{H}}\left(\frac{\partial \mathbf{r}_l'}{\partial \gamma_j}\right),\end{aligned} \tag{42}$$

where γ_p and γ_j represent the pth and jth elements of $\boldsymbol{\gamma}$, respectively. $(\cdot)^{-\mathrm{T}} = \left(()^{-1}\right)^{-\mathrm{T}}$ and $\mathbf{r}_l = \mathrm{vec}\{\mathbf{R}_l\}$ and $\mathbf{r}_l'$ is given as

$$\mathbf{r}_l' = \left((\mathbf{R}_l)^{-\mathrm{T}/2} \otimes (\mathbf{R}_l)^{-1/2}\right)\mathbf{r}_l, \tag{43}$$

where $(\cdot)^{-\mathrm{T}/2} = \left(()^{-1/2}\right)^{-\mathrm{T}}$.

We define $\mathbf{r}' = \left[\mathbf{r}_1'^{\mathrm{T}}, \cdots, \mathbf{r}_L'^{\mathrm{T}}\right]^{\mathrm{T}}$ as

$$\mathbf{J} = \frac{J}{2}\left(\frac{\partial \mathbf{r}'}{\partial \boldsymbol{\gamma}^{\mathrm{T}}}\right)^{\mathrm{H}}\left(\frac{\partial \mathbf{r}'}{\partial \boldsymbol{\gamma}^{\mathrm{T}}}\right), \tag{44}$$

where

$$\frac{\partial \mathbf{r}'}{\partial \boldsymbol{\gamma}^{\mathrm{T}}} = \left[\frac{\partial \mathbf{r}'}{\partial \mathbf{p}^{\mathrm{T}}}, \frac{\partial \mathbf{r}'}{\partial \boldsymbol{\upsilon}^{\mathrm{T}}}\right]. \tag{45}$$

Furthermore, (44) can be rewritten as follows.

$$\mathbf{J} = \frac{J}{2}\begin{bmatrix}\left(\frac{\partial \mathbf{r}'}{\partial \mathbf{p}^{\mathrm{T}}}\right)^{\mathrm{H}}\frac{\partial \mathbf{r}'}{\partial \mathbf{p}^{\mathrm{T}}} & \left(\frac{\partial \mathbf{r}'}{\partial \mathbf{p}^{\mathrm{T}}}\right)^{\mathrm{H}}\frac{\partial \mathbf{r}'}{\partial \boldsymbol{\upsilon}^{\mathrm{T}}} \\ \left(\frac{\partial \mathbf{r}'}{\partial \boldsymbol{\upsilon}^{\mathrm{T}}}\right)^{\mathrm{H}}\frac{\partial \mathbf{r}'}{\partial \mathbf{p}^{\mathrm{T}}} & \left(\frac{\partial \mathbf{r}'}{\partial \boldsymbol{\upsilon}^{\mathrm{T}}}\right)^{\mathrm{H}}\frac{\partial \mathbf{r}'}{\partial \boldsymbol{\upsilon}^{\mathrm{T}}}\end{bmatrix}. \tag{46}$$

Finally, the CRB, with respect to the source location, can be calculated as

$$\mathrm{CRB}_{\mathbf{p}} = \frac{2}{J}\left\{\left(\frac{\partial \mathbf{r}'}{\partial \mathbf{p}^{\mathrm{T}}}\right)^{\mathrm{H}}\mathbf{P}^{\perp}_{\frac{\partial \mathbf{r}'}{\partial \boldsymbol{\upsilon}^{\mathrm{T}}}}\frac{\partial \mathbf{r}'}{\partial \mathbf{p}^{\mathrm{T}}}\right\}^{-1}, \tag{47}$$

where

$$\mathbf{P}^{\perp}_{\frac{\partial \mathbf{r}'}{\partial \boldsymbol{\upsilon}^{\mathrm{T}}}} = \mathbf{I} - \frac{\partial \mathbf{r}'}{\partial \boldsymbol{\upsilon}^{\mathrm{T}}}\left(\left(\frac{\partial \mathbf{r}'}{\partial \boldsymbol{\upsilon}^{\mathrm{T}}}\right)^{\mathrm{H}}\frac{\partial \mathbf{r}'}{\partial \boldsymbol{\upsilon}^{\mathrm{T}}}\right)^{-1}\left(\frac{\partial \mathbf{r}'}{\partial \boldsymbol{\upsilon}^{\mathrm{T}}}\right)^{\mathrm{H}}, \tag{48}$$

$$\frac{\partial \mathbf{r}'}{\partial \mathbf{p}^{\mathrm{T}}} = \begin{bmatrix}\frac{\partial \mathbf{r}_1'}{\partial \mathbf{p}^{\mathrm{T}}} \\ \vdots \\ \frac{\partial \mathbf{r}_L'}{\partial \mathbf{p}^{\mathrm{T}}}\end{bmatrix} = \begin{bmatrix}\frac{\partial \mathbf{r}_1'}{\partial \mathbf{p}_x^{\mathrm{T}}} & \frac{\partial \mathbf{r}_1'}{\partial \mathbf{p}_y^{\mathrm{T}}} \\ \vdots & \vdots \\ \frac{\partial \mathbf{r}_L'}{\partial \mathbf{p}_x^{\mathrm{T}}} & \frac{\partial \mathbf{r}_L'}{\partial \mathbf{p}_y^{\mathrm{T}}}\end{bmatrix}, \tag{49}$$

$$\frac{\partial \mathbf{r}'}{\partial \boldsymbol{\upsilon}^{\mathrm{T}}} = \begin{bmatrix}\frac{\partial \mathbf{r}_1'}{\partial \boldsymbol{\upsilon}^{\mathrm{T}}} \\ \vdots \\ \frac{\partial \mathbf{r}_L'}{\partial \boldsymbol{\upsilon}^{\mathrm{T}}}\end{bmatrix} = \begin{bmatrix}\frac{\partial \mathbf{r}_1'}{\partial \boldsymbol{\Phi}^{\mathrm{T}}} & \frac{\partial \mathbf{r}_1'}{\partial \boldsymbol{\eta}^{\mathrm{T}}} & \frac{\partial \mathbf{r}_1'}{\partial \sigma_{\mathrm{n}}^2} \\ \vdots & \vdots & \vdots \\ \frac{\partial \mathbf{r}_L'}{\partial \boldsymbol{\Phi}^{\mathrm{T}}} & \frac{\partial \mathbf{r}_L'}{\partial \boldsymbol{\eta}^{\mathrm{T}}} & \frac{\partial \mathbf{r}_L'}{\partial \sigma_{\mathrm{n}}^2}\end{bmatrix}. \tag{50}$$

4.2 | Degree of freedom and complexity analysis

Compared with conventional location and tracking methods for circular signals, the degree of freedom of the NC signal is twice as high, thus implying that under the same conditions, the NC method can monitor more sources. Thus, we calculate the computational complexity of the proposed method and compare the results to two-step-MUSIC, two-step-ESPRIT, and reduced dimension (RD)-DPD algorithms. The two-step algorithms are based on the contemporary MUSIC [28] and ESPRIT [29]

algorithms, which calculate the DOA in the first step. In the second step, both algorithms obtain the signal location by clustering intersections. The RD-DPD algorithm [30] is an improved DPD algorithm that uses NC characteristics with an RD concept. Furthermore, the nearest neighbor association method is used to associate algorithmic data for comparison. We use the number of complex multiplications as a standard measure of complexity. Table 1 lists the specific complexities of these algorithms, where N_θ and N_φ are the numbers of search grids for the angle and NC phases, respectively; and n is the number of search grids on the coordinate axes of the RD-DPD algorithm.

To intuitively demonstrate the superiority of the proposed method, Figure 2 demonstrates the computational complexity of the four algorithms with different array element number settings, where $N_S = 60$, $L = 4$, $J = 200$, $K = 2$, $N_\theta = 180$, $N_\varphi = 90$, and $n = 1000$. It is obvious that the proposed method has a significant advantage in terms of complexity over the two-step MUSIC and RD-DPD algorithms because it avoids a grid search. The performance of the proposed method was only slightly better than that of the two-step ESPRIT algorithm because we used the number of complex multiplications as the calculation criterion for complexity. However, in practice, the proposed algorithm still has greater advantages than the two-step algorithm because it requires a new mathematical model to calculate intersections and clusters, which considerably reduces the computational burden of real-number multiplications.

4.3 | Simulation analysis

This subsection describes the experiments conducted to simulate the DPT problem. In our experiments, we initially considered whether the proposed method could effectively track sources under harsh conditions, such as source trajectory crossovers and multiple sources whose motion trajectories satisfy different models. Assuming that source state $\mathbf{x}_{k,t} = \left(x_{k,t}, \dot{x}_{k,t}, \ddot{x}_{k,t}, y_{k,t}, \dot{y}_{k,t}, \ddot{y}_{k,t}\right)^{\mathrm{T}}$ satisfies a constant acceleration (CA) model,

$$\mathbf{x}_{k,t+1} = \mathbf{F}\mathbf{x}_{k,t} + \mathbf{G}\mathbf{v}_k, \tag{51}$$

where $\dot{x}_{k,t}$ and $\dot{y}_{k,t}$ are velocities (m/s) on the x and y axes, respectively, and $\ddot{x}_{k,t}$ and $\ddot{y}_{k,t}$ are the corresponding accelerations (m/s^2). $\mathbf{F}$ is the transition matrix, which is obtained as

$$\mathbf{F} = \begin{bmatrix} \mathbf{F}_T & \mathbf{O}_{3\times3} \\ \mathbf{O}_{3\times3} & \mathbf{F}_T \end{bmatrix}, \tag{52}$$

where

$$\mathbf{F}_T = \begin{bmatrix} 1 & \Delta T & \Delta T^2/2 \\ 0 & 1 & \Delta T \\ 0 & 0 & 1 \end{bmatrix}, \tag{53}$$

and coefficient matrix $\mathbf{G}$ is defined as

$$\mathbf{G} = \begin{bmatrix} \mathbf{G}_T & \mathbf{O}_{3\times1} \\ \mathbf{O}_{3\times1} & \mathbf{G}_T \end{bmatrix}, \tag{54}$$

where

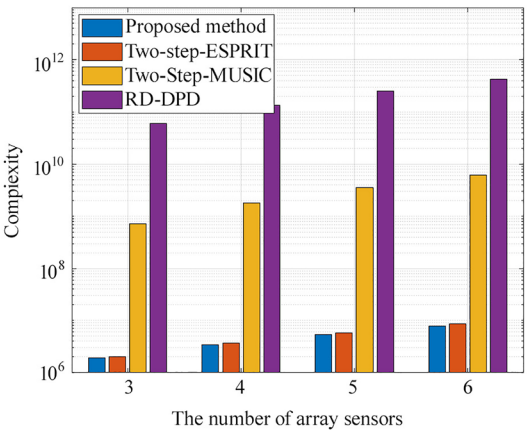

FIGURE 2 Computational complexity of the four approaches.

TABLE 1 Complexity comparison.

Algorithms	Complexity
Two-step-MUSIC	$O\left(N_S L\left(4M^2J + 8M^3 + N_\theta N_\varphi\left(8M^3 - 4M^2K + 4M^2 + 2M\right)\right)\right)$
Two-step-ESPRIT	$O\left(N_S L\left(4M^2J + 8M^3 + 8M^3K + 6MK^2 + 16M^2K + 8K^3\right)\right)$
RD-DPD	$O\left(N_S L\left(4M^2J + 8M^3 + n^2\left(8M^3 - 4M^2K + 8M^2 + 8M + 14\right)\right)\right)$
Proposed method	$O\left(N_S L\left(4M^2J + 8M^3 + 16M^2K + 16MK^2 - 9K^3 - 3K^2\right)\right)$

$$\mathbf{G}_T = \begin{bmatrix} \Delta T^2/2 \\ \Delta T \\ 1 \end{bmatrix}. \tag{55}$$

$\Delta T = 1$ s denotes the time step, and $\mathbf{v}_k$ denotes a zero-mean Gaussian process. Four observation stations were placed at $(0, 0)$, $(0, 1000m)$, $(1000m, 0)$, and $(1000m, 1000m)$.

Figure 3 shows the tracking results of the proposed method when the trajectories cross, where N_S is 60 s, the number of array elements is $M = 8$, the number of snapshots is $J = 200$, SNR = 15 dB, and $K = 2$. The initial source target states are $\mathbf{x}_{1,1} = (108, 8, 0, 792, -8, 0)^{\mathrm{T}}$, and $\mathbf{x}_{2,1} = (108,8,0,400.1,0,0.2)^{\mathrm{T}}$. This demonstrates that the proposed method can effectively and accurately track multiple sources using OLS to handle trajectory crossing. Figure 4 illustrates the tracking results of multiple sources satisfying different moving models, where $K = 4$. Evidently, the proposed method efficiently tracked multiple sources that satisfied different movement models.

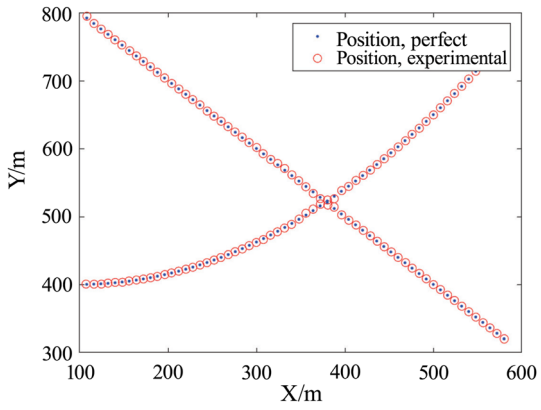

FIGURE 3 Tracking results when trajectories cross.

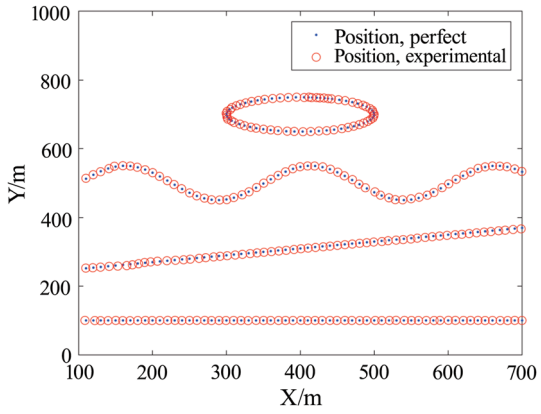

FIGURE 4 Tracking results of multiple sources.

In the next simulations, we compare the proposed method with several approaches, including the two-step MUSIC algorithm, two-step ESPRIT algorithm, RD-DPD algorithm, NC-particle filter (PF) algorithm, NC-Kalman filter (KF) algorithm, the proposed method for circular signals (PMC), and CRB. The NC-PF algorithm is a direct tracking method based on the PF [31], which replaces its own likelihood function with the cost function in the RD-DPD algorithm. It obtains the positions of the sources and achieves tracking via the weighted summation of particles. The NC-KF algorithm, an improvement on the two-step ESPRIT algorithm, optimizes the tracking trajectory using the KF [32] algorithm. The root-mean-square error (RMSE) was used to evaluate the tracking performance. It is expressed as follows.

$$\mathrm{RMSE} = \sqrt{\frac{1}{CN_SK}\sum_{c=1}^{C}\sum_{t=1}^{N_S}\sum_{k=1}^{K}||\tilde{\mathbf{p}}_{k,t}^{c} - \mathbf{p}_{k,t}||^2}, \tag{56}$$

where $\tilde{\mathbf{p}}_{k,t}^{c}$ is the estimate of $\mathbf{p}_{k,t}$ from the cth Monte Carlo trial at time t. The parameters were set to $K = 2$ and $C = 100$, and the initial source target states were $\mathbf{x}_{1,1} = (100, 8, 0, 100, 8, 0)^{\mathrm{T}}$ and $\mathbf{x}_{2,1} = (100, 8, 0, 400, 0, 0.2)^{\mathrm{T}}$. The other parameters were identical to those used in the previous simulations.

Figure 5 shows the RMSE of each algorithm at different SNRs. The proposed method shows considerable improvements in performance compared with the other algorithms. Even at a low SNR, the proposed method performs well and accurately tracks the sources. By leveraging the unique characteristics of NC signals, the proposed method demonstrates improved performance in terms of accuracy, robustness, and resilience in challenging wireless environments. The results were combined with those of the previous complexity analysis and clearly revealed

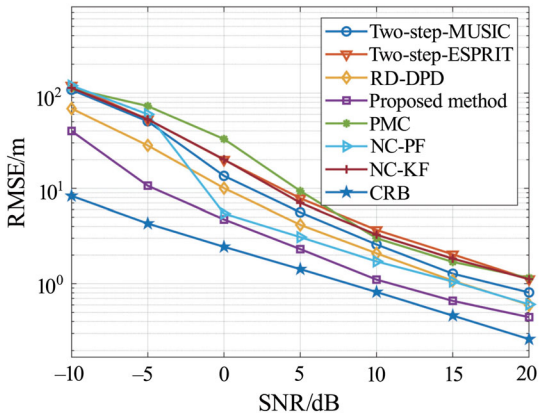

FIGURE 5 Tracking performance comparisons (SNR).

that the proposed method is superior in both aspects, owing to the joint processing of the signal subspaces received from multiple observation stations and the use of information from previous iterations. Figure 6 displays the effects of different numbers of snapshots on RMSE, where SNR = 15 dB. This shows that the proposed method becomes increasingly effective as the number of snapshots increases, and the proposed method has advantages over the other algorithms, regardless of the number of snapshots. Moreover, in both simulations, the proposed method is the closest to CRB.

To illustrate the performance superiority of the algorithm another way, we redefine the RMSE at each time point as

$$\mathrm{RMSE}(t) = \sqrt{\frac{1}{CK}\sum_{c=1}^{C}\sum_{k=1}^{K}||\tilde{\mathbf{p}}_{k,t}^{c} - \mathbf{p}_{k,t}||^2}. \quad (57)$$

Figures 7 and 8 show the tracking history of the RMSE when SNR = −5 and 10 dB, respectively, where $J = 200$ and $N_S = 30$ s. This reveals that the proposed method can accurately track signals every time and has high precision at a low SNRs. A comparison with other algorithms shows that the proposed method outperforms them every time, and the performance does not change significantly with a change in signal location. Therefore, the proposed method is more robust.

For the final simulation, we considered the tracking effects of the proposed method for different numbers of array elements. The results are presented in Figure 9, and the RMSE was calculated according to (56). Evidently, the performance of the proposed algorithm improved as the number of arrays increased. When the number of arrays was small, an increase in the number of arrays had a greater impact on performance, and a continued increase in the number of arrays had a smaller impact.

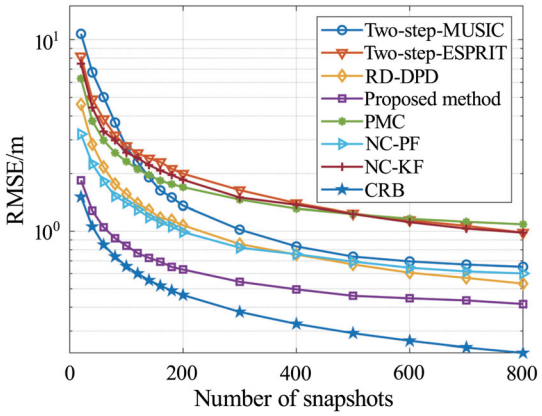

FIGURE 6 Tracking performance comparison of different snapshots.

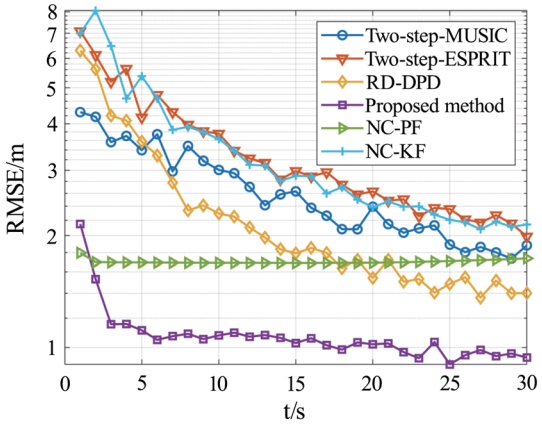

FIGURE 8 Tracking performance comparison of history (SNR = 10 dB).

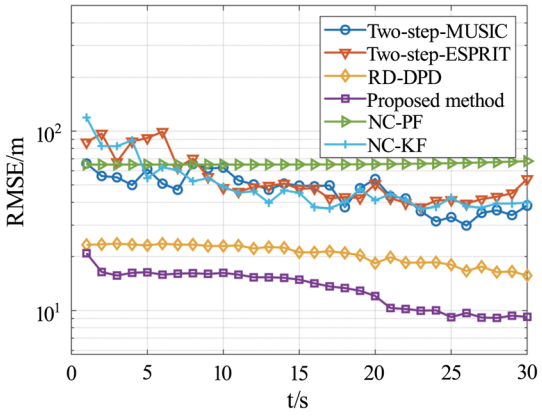

FIGURE 7 Tracking performance comparison of history (SNR = −5 dB).

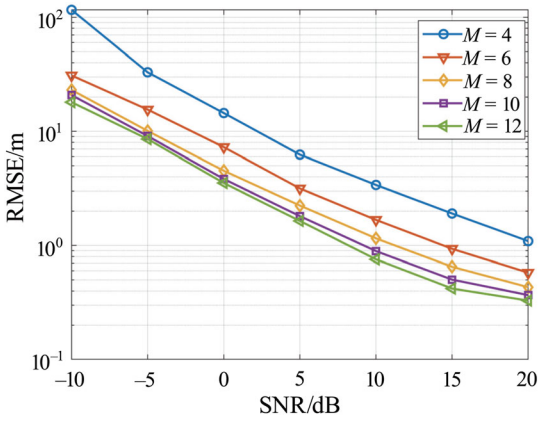

FIGURE 9 Tracking performance for different numbers of array elements.

5 | CONCLUSION

In this study, we proposed a DPT method for moving NC signals using a first-order approximation, which achieves excellent performance and robustness. By fusing the subspace and transforming the tracking into first-order approximation iterations, the problems of building a new geometric model and grid searching were avoided, thereby improving the accuracy of the proposed algorithm compared with others. The proposed method avoids traditional association processes and directly resolves target signal locations, thus outperforming other algorithms in terms of complexity. Numerous simulation results demonstrated the advantages of the proposed method. We plan to delve deeper into the properties of sparse arrays to further upgrade the algorithm.

CONFLICT OF INTEREST STATEMENT

The authors declare that there are no conflicts of interest.

ORCID

Jinke Cao https://orcid.org/0000-0002-8033-0960
Honghao Hao https://orcid.org/0009-0000-4225-359X

REFERENCES

1. Z. Tang and A. Manikas, *Multi direction-of-arrival tracking using rigid and flexible antenna arrays*, IEEE Trans. Wireless. Commun. **20** (2021), 7568–7580. https://doi.org/10.1109/TWC.2021.3085753
2. C. Liu, M. Li, L. Zhao, P. Whiting, S. V. Hanly, I. B. Collings, and M. Zhao, *Robust adaptive beam tracking for mobile millimeter wave communications*, Trans. Wireless. Commun. **20** (2021), 1918–1934. https://doi.org/10.1109/TWC.2020.3037552
3. H. Ye, B. Yang, Z. Long, and C. Dai, *A method of indoor positioning by signal fitting and PDDA algorithm using BLE AOA device*, IEEE Sensors J. **22** (2022), 7877–7887. https://doi.org/10.1109/JSEN.2022.3141739
4. M. Wagner, Y. Park, and P. Gerstoft, *Gridless DOA estimation and root-MUSIC for non-uniform linear arrays*, IEEE Trans. Signal Proc. **69** (2021), 2144–2157. https://doi.org/10.1109/TSP.2021.3068353
5. L. Xu, J. Lien, and J. Li, *Doppler-range processing for enhanced high-speed moving target detection using LFMCW automotive radar*, IEEE Trans. Aerosp. Electron. Sys. **58** (2022), 568–580. https://doi.org/10.1109/TAES.2021.3101768
6. Q. Li, B. Chen, and M. Yang, *Improved two-step constrained total least-squares TDOA localization algorithm based on the alternating direction method of multipliers*, IEEE Sensors J. **20** (2020), 13666–13673. https://doi.org/10.1109/JSEN.2020.3004235
7. F. Ma, Z. M. Liu, and F. Guo, *Direct position determination in asynchronous sensor networks*, IEEE Trans. Vehic. Technol. **68** (2019), 8790–8803. https://doi.org/10.1109/TVT.2019.2928638
8. L. Wang, Y. Yang, and X. Liu, *A direct position determination approach for underwater acoustic sensor networks*, IEEE Trans. Vehic. Technol. **69** (2020), 13033–13044. https://doi.org/10.1109/TVT.2020.3018489
9. T. Tirer and A. J. Weiss, *Performance analysis of a high-resolution direct position determination method*, IEEE Trans. Signal Proc. **65** (2017), 544–554. https://doi.org/10.1109/TSP.2016.2621729
10. A. J. Weiss, *Direct position determination of narrowband radio frequency transmitters*, IEEE Signal Proc. Let. **11** (2004), 513–516. https://doi.org/10.1109/LSP.2004.826501
11. B. Demissie, M. Oispuu, and E. Ruthotto, Localization of multiple sources with a moving array using subspace data fusion, (Proc. 11th Int. Conf. Informat. Fusion, IEEE, Cologne, Germany), 2008, pp. 1–7.
12. Z. Wang, K. Hao, Y. Sun, L. Xie, and Q. Wan, *A computationally efficient direct position determination algorithm based on OFDM system*, IEEE Commun. Let. **27** (2023), 841–845. https://doi.org/10.1109/LCOMM.2022.3231548
13. F. Ma, F. Guo, and L. Yang, *Direct position determination of moving sources based on delay and Doppler*, IEEE Sensors J. **20** (2020), 7859–7869. https://doi.org/10.1109/JSEN.2020.2980012
14. F. Ma, Z. M. Liu, and F. Guo, *Distributed direct position determination*, IEEE Trans. Vehic. Technol. **69** (2020), 14007–14012. https://doi.org/10.1109/TVT.2020.3025386
15. T. Tirer and A. J. Weiss, *High resolution direct position determination of radio frequency sources*, IEEE Signal Proc. Let. **23** (2016), 192–196. https://doi.org/10.1109/LSP.2015.2503921
16. J. S. Picard and A. J. Weiss, *Direct position determination sensitivity to NLOS propagation effects on Doppler-shift*, IEEE Tans. Signal Proc. **67** (2019), 3870–3881. https://doi.org/10.1109/TSP.2019.2923152
17. L. Steinweg, J. Hebeler, T. Meister, T. Zwick, and F. Ellinger, *8.0-pJ/bit BPSK transmitter with LO phase steering and 52-Gbps data rate operating at 246 GHz*, IEEE Trans. Microw. Theory Techniq. **71** (2023), no. 7, 3217–3226. https://doi.org/10.1109/TMTT.2023.3239792
18. R. K. Mallik and R. Murch, *Channel norm based energy detection with diversity reception for amplitude-shift keying in Rayleigh fading*, IEEE Trans. Wireless Commun. **22** (2023), 5855–5870. https://doi.org/10.1109/TWC.2023.3237932
19. J. Yin, Y. Wu, and D. Wang, *Direct position determination of multiple noncircular sources with a moving array*, Cir. Sys. Signal Proc. **36** (2017), 4050–4076.
20. Y. Zhang, B. Ba, D. Wang, W. Geng, and H. Xu, *Direct position determination of multiple noncircular sources with moving coprime array*, Sensors **18** (2018), 1479.
21. G. Kumar, P. Ponnusamy, and I. Sadegh Amiri, *Direct localization of multiple noncircular sources with a moving nested array*, IEEE Access **7** (2019), 101106–101116. https://doi.org/10.1109/ACCESS.2019.2929805
22. J. Deng, J. Yin, B. Yang, and D. Wang, *Direct position determination algorithm for non-circular sources in the presence of mutual coupling and its theoretical performance analysis*, IET Signal Proc. **17** (2023), e12193.
23. X. Zhang, W. Chen, W. Zheng, Z. Xia, and Y. Wang, *Localization of near-field sources: a reduced-dimension MUSIC algorithm*, IEEE Commun. Let. **22** (2018), 1422–1425. https://doi.org/10.1109/LCOMM.2018.2837049
24. Z. Li, X. Zhang, and J. Shen, *2D-DOA estimation of strictly noncircular sources utilizing connection-matrix for L-shaped array*,

IEEE Wireless Commun. Let. **10** (2021), 296–300. https://doi.org/10.1109/LWC.2020.3029457
25. H. Abeida and J. P. Delmas, *MUSIC-like estimation of direction of arrival for noncircular sources*, IEEE Trans. Signal Proc. **54** (2006), 2678–2690. https://doi.org/10.1109/TSP.2006.873505
26. H. Abeida and J. P. Delmas, *Direct derivation of the stochastic CRB of DOA estimation for rectilinear sources*, IEEE Signal Proc. Let. **24** (2017), 1522–1526. https://doi.org/10.1109/LSP.2017.2744673
27. J. P. Delmas and H. Abeida, *Stochastic Crame/spl acute/r-Rao bound for noncircular signals with application to DOA estimation*, IEEE Trans. Signal Proc. **52** (2004), 3192–3199. https://doi.org/10.1109/TSP.2004.836462
28. L. Wan, K. Liu, Y. C. Liang, and T. Zhu, *DOA and polarization estimation for non-circular signals in 3-D millimeter wave polarized massive MIMO systems*, IEEE Trans. Wireless Commun. **20** (2021), 3152–3167. https://doi.org/10.1109/TWC.2020.3047866
29. Q. Wang, X. Wang, and H. Chen, *DOA estimation algorithm for strictly noncircular sources with unknown mutual coupling*, IEEE Commun. Let. **23** (2018), 2215–2218. https://doi.org/10.1109/LCOMM.2019.2947424
30. Y. Qian, D. Zhao, and H. Zeng, *Direct position determination of noncircular sources with multiple nested arrays: reduced-dimension subspace data fusion*, Wirel. Commun. Mobile Comput. **2021** (2021), 1–10.
31. F. Dong, L. Xu, and X. Li, *Particle filter algorithm for DOA tracking using co-prime array*, IEEE Commun. Let. **24** (2020), 2493–2497. https://doi.org/10.1109/LCOMM.2019.2953466
32. S. R. Jondhale and R. S. Deshpande, *Kalman filtering framework-based real time target tracking in wireless sensor networks using generalized regression neural networks*, IEEE Sensors J. **19** (2019), 224–233. https://doi.org/10.1109/JSEN.2018.2873357

AUTHOR BIOGRAPHIES

Jinke Cao received his B.S. degree in Communication Engineering from Shandong University of Science and Technology, Qingdao, China, in 2020. He is currently working toward a Ph.D. degree in Electronic and Communication Engineering at Nanjing University of Aeronautics and Astronautics, Nanjing, China. His research interests include signal and information processing and radiation source position tracking.

Xiaofei Zhang received his M.S degree in Electrical Engineering from Wuhan University, Wuhan, China, in 2001, and his Ph.D. degree in Communication and Information Systems from the Nanjing University of Aeronautics and Astronautics, Nanjing, China, in 2005.

Honghao Hao received his B.S. degree from Shandong University, Weihai, China, in 2021. He is currently working toward an M.S. degree in Electronic and Communication Engineering at Nanjing University of Aeronautics and Astronautics, Nanjing, China. His research interests include array signal processing and direct position determination.

How to cite this article: J. Cao, X. Zhang, and H. Hao, *Direct position tracking method for non-circular signals with distributed passive arrays via first-order approximation*, ETRI Journal **46** (2024), 421–431. DOI 10.4218/etrij.2023-0075